Thin-Film Electrodes

DOI: 10.1002/anie.201209413

Catalytic Activity of Pt/TaB_2(0001) for the Oxygen Reduction Reaction

Eishiro Toyoda, Ryosuke Jinnouchi, Tetsu Ohsuna, Tatsuya Hatanaka, Takashi Aizawa, Shigeki Otani, Yoshiaki Kido, and Yu Morimoto*

Proton-exchange-membrane fuel cells (PEMFCs) are a promising power source for automobiles. For their wide application, however, there still remain several problems.[1,2] One problem is the limited mass activity (reaction rate per mass) of cathode electrocatalysts for the oxygen reduction reaction (ORR). Bulk Pt has a high specific activity (reaction rate per surface area), and the specific activity can be further increased by alloying the subsurfaces with several nonprecious metals, such as Fe, Co, Ni, Cu, Sc, or Y,[3–7] or by replacing subsurfaces with Pd.[8] However, the specific areas (surface area per mass of the precious metal) of bulk materials are small, and therefore, the mass activities (specific activity multiplied by specific area) are also small. To increase the mass activity, the specific surface area should be increased by decreasing the catalyst size to the nanometer scale. Although Pt nanoparticles supported on carbon (Pt/C) are used practically in PEMFCs,[1] the mass activity is not sufficiently high because the decrease in the size of the catalyst leads to a decrease in the specific activity as a result of the so-called particle-size effect.[1,9,10] To avoid the particle-size effect, the specific surface area must be increased while maintaining the extended bulklike surface morphology. This new approach was employed by the company 3M in the development of nanostructured thin-film (NSTF) catalysts, in which Pt films with a thickness of a few tens of nanometers are deposited on organic nanostructured whiskerlike supports.[11] The discovery of these new electrocatalysts inspired a number of studies on the fabrication of electrocatalysts with an extended Pt surface and high specific surface area with the aim of further increasing the mass activity.[12–14]

Herein, we show that a high mass activity of 1890 $A\,g^{-1}$, which is six times as high as that of Pt/C (299 $A\,g^{-1}$), can be attained by the use of an epitaxial Pt thin film with a thickness of 1.5 nm on a TaB_2(0001) single-crystal substrate. High-angle annular dark-field scanning transmission electron microscopy (HAADF-STEM) images of the Pt/TaB_2 structure at the $[10\bar{1}0]_{TaB_2}$ incidence and the $[2\bar{1}\bar{1}0]_{TaB_2}$ incidence are shown in Figure 1.

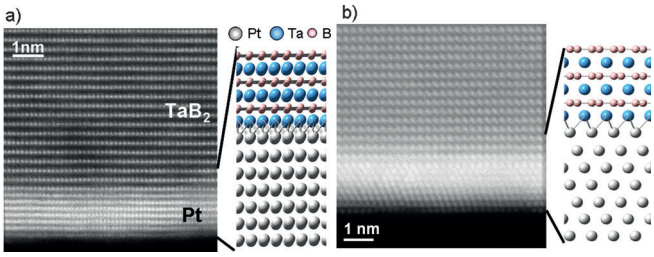

Figure 1. HAADF-STEM images of the epitaxial Pt thin film on the TaB_2(0001) single-crystal substrate as observed for: a) $[10\bar{1}0]_{TaB_2}$ incidence; b) $[2\bar{1}\bar{1}0]_{TaB_2}$ incidence.

TaB_2(0001) was selected because of its strong bonding with Pt, as shown by our DFT calculations, which indicated a cohesive energy of the Pt monolayer on TaB_2(0001) terminated with Ta of 6.47 eV, which is much larger than that of a Pt monolayer on a graphene sheet (3.76 eV) or on Pt(111) (5.06 eV). We deposited Pt on the cleaned TaB_2(0001) substrate and carried out CO annealing[15] to obtain a flat and uniform Pt surface. Figure 2a shows the cyclic voltammogram (CV) recorded during CO annealing. In the anodic scan of the first cycle, the oxidation current appeared at approximately 0.5 V and then gradually increased (preignition potential region). This oxidation current disappeared in following cycles. The oxidation current in the preignition region is due to CO oxidation at the sites of Pt adatoms and adislands; thus, the disappearance of this current suggests the elimination of the Pt adatoms and adislands.[15] Figure 2b shows the voltammogram for CO stripping in an argon-purged solution. The electrochemical surface area (ECSA) was estimated from the charge of 420 $\mu C\,cm^{-2}$ required for CO oxidation to be 0.21 cm^2, which corresponds to a roughness factor (ECSA/geometrical surface area) of 1.06. The ORR activity of the Pt/TaB_2(0001) alloy was evaluated by linear sweep voltammetry with a rotating disk electrode (measurement at 1600 rpm) under oxygen-saturated conditions (Figure 2c). The current on Pt/TaB_2(0001) was corrected to compensate for the geometrical conditions of the working electrode (see Figure S1 in the Supporting Information for details). The specific activity of Pt/TaB_2(0001) (kinetic current at 0.9 V) was 4961 $\mu A\,cm^{-2}$, which is more than twice that observed for polycrystalline Pt (1400 $\mu A\,cm^{-2}$) and Pt(111) (1867 $\mu A\,cm^{-2}$). The mass activity of Pt/TaB_2(0001) was 1890 $A\,g^{-1}$, which is almost six times that of Pt/C (299 $A\,g^{-1}$). The CVs recorded under argon-saturated conditions are shown in Figure 2d. The shape of the CV of Pt/TaB_2(0001) is more similar to that of polycrystalline Pt than to

[*] E. Toyoda, Dr. R. Jinnouchi, Dr. T. Ohsuna, T. Hatanaka, Dr. Y. Morimoto
Toyota Central Research and Development Laboratories, Inc.
Nagakute, Aichi, 480-1192 (Japan)
E-mail: eishirot@mosk.tytlabs.co.jp
Dr. T. Aizawa, Dr. S. Otani
National Institute for Materials Science
1-1 Namiki, Tsukuba, Ibaraki 305-0044 (Japan)
Dr. Y. Kido
Department of Physics, Ritsumeikan University
Kusatsu, Shiga-ken 525-8577 (Japan)

Supporting information for this article is available on the WWW under http://dx.doi.org/10.1002/anie.201209413.

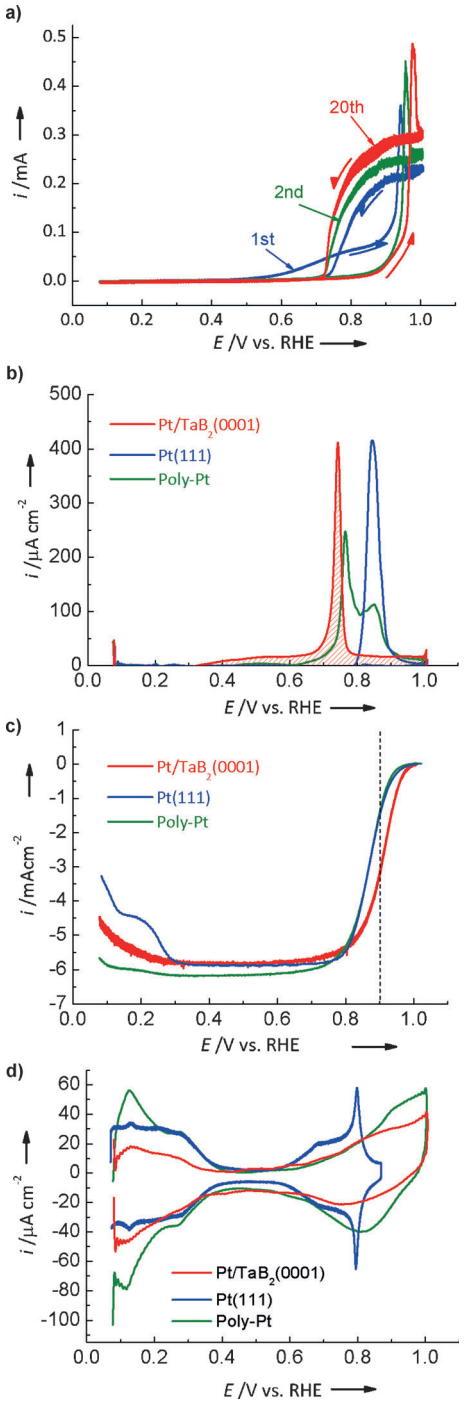

Figure 2. a) Cyclic voltammogram (CV) at 50 mVs^{-1} for $Pt/TaB_2(0001)$ during CO annealing. b) CV for CO stripping, as obtained by subtracting the second-cycle CV from the first-cycle CV profile. c) ORR currents measured for $Pt/TaB_2(0001)$, Pt(111), and polycrystalline Pt (poly-Pt) under oxygen-saturated conditions by linear sweep voltammetry at 10 mVs^{-1} and 1600 rpm. d) CVs measured under argon-saturated conditions for $Pt/TaB_2(0001)$, Pt(111), and polycrystalline Pt after ORR evaluation.

that of Pt(111). From the charge of 210 $\mu C cm^{-2}$ associated with hydrogen desorption, the ECSA was estimated to be 0.059 cm^2, which is a third of that estimated from CO stripping. This result suggests that the Pt layers are alloyed.[16]

We used X-ray photoelectron spectroscopy to determine the electronic state of the Pt 4f core level. The Pt4f(7/2) binding energy was observed at $BE = 71.5$ eV, which is 0.5 eV higher than that of polycrystalline Pt (see Figure S2a) and 0.4 eV higher than that of Pt(111).[17] The surface structure and elements were analyzed by field-emission scanning electron microscopy (FESEM; see Figure S3a,b). Small dark areas were observed and identified as tantalum oxides (TaO_x) without Pt by energy-dispersive X-ray (EDX) analysis. From the SEM images, the areal occupation of TaO_x was estimated to be about 7%. The HAADF-STEM images shown in Figure 1a,b indicate that seven Pt monolayers stack uniformly in the white region of Figure S3a (see the Supporting Information). The Pt layer was regarded as an fcc crystal on the basis of images obtained with two incidence directions. The lattice constant of the fcc crystal was estimated from the images to be 0.40 nm, which is close to that of the Pt crystal (0.392 nm). The incidence directions were determined to be $[211]_{fcc}$ for Figure 1a and $[110]_{fcc}$ for Figure 1b. EDX line analysis showed that the Pt layers contain Ta (Figure 3a,b). Boron was not observed in the thin layer and therefore seems to have no effect on the properties of the thin layer. The elemental composition of the Pt layer varies from 0.70 at the interface to 0.85 on top. This alloying was probably induced during vacuum annealing after Pt deposition. In spite of the high concentration of Ta in the Pt–Ta alloy layer, the interatomic and interlayer distances observed are almost the same as those of bulk Pt.

We carried out DFT calculations to determine the Pt4f-core-level shift and lattice constant of Pt–Ta alloys as a function of Ta concentration. The Pt4f(7/2)-core-level shift of 0.4 eV found for the $Pt_{85}Ta_{15}$ alloy agrees with the experimental results (see Figure S2b). The calculated lattice constant showed an expansion of merely 0.7% at a Ta concentration of 0.5 (see Figure S4), which also agrees with the experimental result obtained by STEM. However, this small expansion strain is not sufficient to explain the enhanced ORR activity of the (Pt–Ta)/TaB_2(0001) material. We therefore consider the enhancement to be caused by the electronic effect of Ta on Pt. Our DFT calculations showed that the Pt monolayer on the $Pt_{85}Ta_{15}$ alloy ($Pt_{ML}/Pt_{85}Ta_{15}$) has a lower d-band center (−2.43 eV) than that of a Pt monolayer on pure Pt (−2.23 eV), and has a smaller O absorption energy and a higher ORR activity than pure Pt (Figure 4).

In conclusion, an extended thin film of Pt with a thickness of 1.5 nm on a TaB_2(0001) substrate exhibited an ORR specific activity twice as large as that observed for polycrystalline Pt or Pt(111) and a mass activity six times as large as that of Pt/C. Analysis and DFT calculations showed that the Pt atoms are highly crystallized and alloyed with Ta and that the enhanced activities are due to the electronic effect of Ta on Pt. These results suggest that TaB_2 particles could be a good substrate for Pt thin-layer catalysts for PEMFCs if their surface is (0001) rich and has no oxide.

Experimental Section

The TaB_2(0001) crystal was provided by the National Institute for Materials Science (NIMS). The crystal rod was cut into small pieces

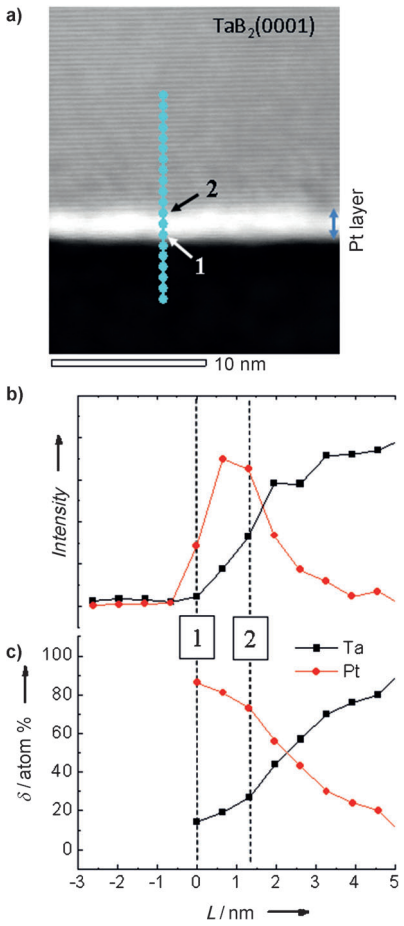

Figure 3. a) HAADF-STEM image of Pt/TaB_2(0001). b) X-ray intensities and c) composition ratio observed by line-scan EDX quantitative analysis (without a standard) as a function of depth. The surface and interface of Pt/TaB_2(0001) are indicated in the image and graphs as 1 and 2, respectively.

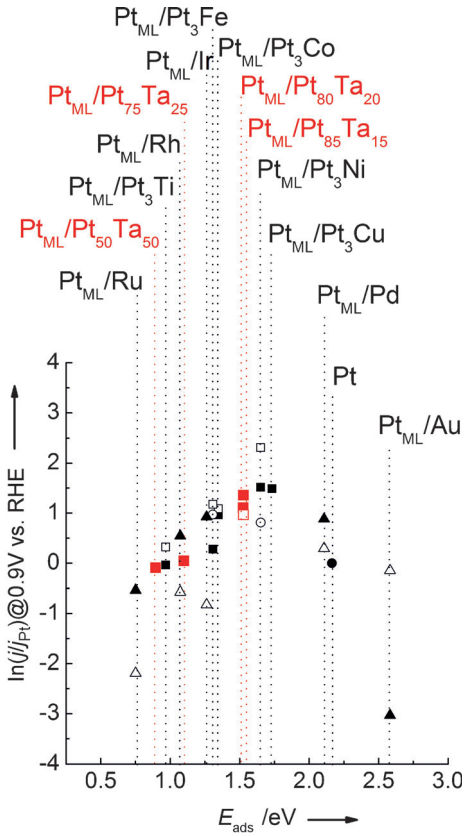

Figure 4. ORR activity expressed as the current at 0.9 V, normalized with respect to the current on bulk Pt, as a function of the oxygen-adsorption energy, E_{ads}, which is defined as the difference in the total energy between an O_2 molecule and two adsorbed oxygen atoms. The red open square for $Pt_{ML}/Pt_{85}Ta_{15}$ is the experimental result, and the filled squares are calculated results. Other open symbols indicate experimental results summarized in Ref. [21], and the other filled symbols are calculated results. Pt_{ML}/ means coverage with one monolayer of Pt.

with a diameter and thickness of 5 and 2 mm, respectively, the surface of which was then mechanically polished to a mirror finish. After chemical treatment, the surface was cleaned by an annealing method reported by H. Kawanowa et al.,[18] and then Pt was deposited (8.1×10^{15} atoms cm^{-2}) on the surface at room temperature by vacuum deposition. The sample was annealed at 1000 °C for 5 min in an ultrahigh vacuum.

Electrochemical evaluation was carried out with a rotating disk electrode (RDE) combined with a potentiostat. Gold wire and Ag/AgCl were used as the counter and reference electrode, respectively. The reference electrode was calibrated with a reversible hydrogen electrode (RHE). First, a CV was measured in an argon-saturated electrolyte solution, and the bubbling gas was then changed to carbon monoxide for CO annealing. The gas was then switched back from CO to Ar to measure CO stripping. The ORR activity was measured under oxygen-saturated conditions by linear sweep voltammetry at 10 mV s^{-1} and 1600 rpm. Finally, CVs were recorded under argon-saturated conditions. TEM was carried out at 200 kV with a JEOL JEM-2100F microscope with a Cs corrector. The electronic state of Pt4f in Pt/TaB_2(0001) was measured with $Al_{K\alpha}=1.49$ keV with a PHI Quantera SXM instrument.

Theoretical methods: The DFT calculations were carried out with triple-zeta plus polarization basis sets for H and O and double-zeta plus polarization basis sets for Pt and Ta. The exchange-correlation functional was described by a revised Perdew–Burke–Ernzerhof-type generalized gradient approximation,[19] and ionic cores were described by Troullier–Martins-type norm-conserving pseudopotentials.[20] A 2×2 periodicity was used to describe extended surfaces, and Brillouin zone integrations were carried out with a 5×5 uniform k-point mesh and a Gaussian smearing with an energy width of 0.1 eV.[21] All total energies were extrapolated to $k_B T=0$ eV. In the calculations of the cohesive energy of Pt monolayers, TaB_2(0001) was modeled as a three-layer slab, and Pt(111) was modeled as a five-layer slab. The model of a graphene sheet is the same as that used by us in a previous study.[22] In the calculations of the d-band centers of the Pt monolayers and the adsorption energies of reaction intermediates O, OH, and HOO, surfaces were modeled as Pt monolayers on five-layer slabs of $Pt_{50}Ta_{50}$, $Pt_{75}Ta_{25}$, $Pt_{80}Ta_{20}$, and $Pt_{85}Ta_{15}$ alloys, the structures of which are shown in the Supporting Information (Figures S5–S8). In the calculations of the d-band centers, spin–orbit coupling was included within a perturbation approximation, and projected state densities were integrated up to 15 eV above the Fermi energies. The obtained d-band centers were averaged over all surface Pt atoms and used as an indicator of the ORR activity. In the calculations of the adsorption energies, in similar approach to that used in previous theoretical studies,[3,7] the most stable adsorption sites and adsorbate structures were explored, and those adsorption energies were used to calculate the ORR activity. The adsorption energies were converted into the specific ORR activity by the method described in Ref. [23]. The ORR activity was plotted as $\ln(j/j_{Pt})$ at 0.9 V versus the O

absorption energy, E_{ads}, and compared with the data reported by Rossmeisl and Nørskov[24] and past calculation results for other alloys and pure Pt by Jinnouchi et al.[23] As in past theoretical studies,[23,25] E_{ads} was obtained from the total energy of molecular oxygen as calculated from the total energies of hydrogen and water molecules and the empirical formation energy of a water molecule. Pt4f-core-level shifts were calculated by the use of pseudopotentials with core holes.[26] In this calculation, a slab comprised of five layers of pure Pt and five layers of the Pt–Ta alloy was placed in a vacuum, and the core-level shift was obtained as the energy difference between the slab with a 4f core hole in the bulk layer of pure Pt and that with a 4f core hole in the bulk layer of the Pt–Ta alloy.

Received: November 26, 2012
Published online: March 12, 2013

Keywords: alloys · fuel cells · platinum · tantalum · thin-film electrodes

[1] H. A. Gasteiger, S. S. Kocha, B. Sompalli, F. T. Wagner, *Appl. Catal. B* **2005**, *56*, 9.
[2] F. T. Wagner, B. Lakshmanan, M. F. Mathias, *J. Phys. Chem. Lett.* **2010**, *1*, 2204.
[3] V. Stamenkovic, B. S. Mun, K. J. J. Mayrhofer, P. N. Ross, N. M. Markovic, J. Rossmeisl, J. Greeley, J. K. Nørskov, *Angew. Chem.* **2006**, *118*, 2963; *Angew. Chem. Int. Ed.* **2006**, *45*, 2897.
[4] V. R. Stamenkovic, B. S. Mun, M. Arenz, K. J. J. Mayrhofer, C. A. Lucas, G. Wang, P. N. Ross, N. M. Markovic, *Nat. Mater.* **2007**, *6*, 241.
[5] V. R. Stamenkovic, B. Fowler, B. S. Mun, G. Wang, P. N. Ross, C. A. Lucas, N. M. Markovic, *Science* **2007**, *315*, 493.
[6] J. Greeley, I. E. L. Stephens, A. S. Bondarenko, T. P. Johansson, H. A. Hansen, T. F. Jaramillo, J. Rossmeisl, I. Chorkendorff, J. K. Nørskov, *Nat. Chem.* **2009**, *1*, 552.
[7] I. E. L. Stephens, A. S. Bondarenko, F. J. Perez-Alonso, F. Calle-Vallejo, L. Bech, T. P. Johansson, A. K. Jepsen, R. Frydendal, B. P. Knudsen, J. Rossmeisl, I. Chorkendorff, *J. Am. Chem. Soc.* **2011**, *133*, 5485.
[8] J. Zhang, M. B. Vukmirovic, Y. Xu, M. Mavrikakis, R. R. Adzic, *Angew. Chem.* **2005**, *117*, 2170; *Angew. Chem. Int. Ed.* **2005**, *44*, 2132.
[9] F. J. Perez-Alonso, D. N. McCarthy, A. Nierhoff, P. Hernandez-Fernandez, C. Strebel, I. E. L. Stephens, J. H. Neilsen, I. Chorkendorff, *Angew. Chem.* **2012**, *124*, 4719; *Angew. Chem. Int. Ed.* **2012**, *51*, 4641.
[10] M. Nesselberger, S. Ashton, J. C. Meier, I. Katsounaros, K. J. J. Mayrhofer, M. Arenz, *J. Am. Chem. Soc.* **2011**, *133*, 17428.
[11] M. K. Debe, *Nature* **2012**, *486*, 43.
[12] J. Snyder, T. Fujita, M. W. Chen, J. Erlebacher, *Nat. Mater.* **2010**, *9*, 904.
[13] S. M. Alia, C. Zhang, D. Kisailus, D. Li, S. Gu, K. Jensen, Y. Yan, *Adv. Funct. Mater.* **2010**, *20*, 3742.
[14] S. M. Alia, K. O. Jensen, B. S. Pivovar, Y. Yan, *ACS Catal.* **2012**, *2*, 858.
[15] D. S. Strmcnik, D. V. Tripkovic, D. van der Vliet, K.-C. Chang, V. Komanicky, H. You, G. Karapetrov, J. P. Greeley, V. R. Stamenkovic, N. M. Markovic, *J. Am. Chem. Soc.* **2008**, *130*, 15332.
[16] D. F. van der Vliet, C. W. D. Li, A. P. Paulikas, J. Greeley, R. B. Rankin, D. Strmcnik, D. Tripkovic, N. M. Markovic, V. R. Stamenkovic, *Angew. Chem.* **2012**, *124*, 3193; *Angew. Chem. Int. Ed.* **2012**, *51*, 3139.
[17] R. C. Baetzold, G. Apai, E. Shustorovich, *Phys. Rev. B* **1982**, *26*, 4022.
[18] H. Kawanowa, R. Souda, S. Otani, Y. Gotoh, *Phys. Rev. Lett.* **1998**, *81*, 2264.
[19] B. Hammer, L. B. Hansen, J. K. Nørskov, *Phys. Rev. B* **1999**, *59*, 7413.
[20] N. Troullier, J. L. Martins, *Phys. Rev. B* **1991**, *43*, 1993.
[21] C.-L. Fu, K.-M. Ho, *Phys. Rev. B* **1983**, *28*, 5480.
[22] R. Jinnouchi, E. Toyoda, T. Hatanaka, Y. Morimoto, *J. Phys. Chem. C* **2010**, *114*, 17557.
[23] R. Jinnouchi, K. Kodama, T. Hatanaka, Y. Morimoto, *Phys. Chem. Chem. Phys.* **2011**, *13*, 21070.
[24] J. Rossmeisl, J. K. Nørskov, *Surf. Sci.* **2008**, *602*, 2337.
[25] J. S. Hummelshøj, J. Blomqvist, S. Datta, T. Vegge, J. Rossmeisl, K. S. Thygesen, A. C. Luntz, K. W. Jacobsen, J. K. Nørskov, *J. Chem. Phys.* **2010**, *132*, 071101.
[26] E. Pehlke, M. Scheffler, *Phys. Rev. Lett.* **1993**, *71*, 2338.

